Available online at www.sciencedirect.com
ScienceDirect
Computers and Electrical Engineering 33 (2007) 48–57
Computers and Electrical Engineering
www.elsevier.com/locate/compeleceng

3D depth estimation for visual inspection using wavelet transform modulus maxima

Asim Bhatti [a,b], Saeid Nahavandi [b,*], Yakov Frayman [a,b]

[a] CRC for CAST Metals Manufacturing, Deakin University, Geelong 3217, Australia
[b] Intelligent Systems Research Lab., Deakin University, Vic 3217, Australia

Received 13 October 2005; accepted 18 April 2006
Available online 17 August 2006

Abstract

A vision based approach for calculating accurate 3D models of the objects is presented. Generally industrial visual inspection systems capable of accurate 3D depth estimation rely on extra hardware tools like laser scanners or light pattern projectors. These tools improve the accuracy of depth estimation but also make the vision system costly and cumbersome. In the proposed algorithm, depth and dimensional accuracy of the produced 3D depth model depends on the existing reference model instead of the information from extra hardware tools. The proposed algorithm is a simple and cost effective software based approach to achieve accurate 3D depth estimation with minimal hardware involvement. The matching process uses the well-known coarse to fine strategy, involving the calculation of matching points at the coarsest level with consequent refinement up to the finest level. Vector coefficients of the wavelet transform-modulus are used as matching features, where wavelet transform-modulus maxima defines the shift invariant high-level features with phase pointing to the normal of the feature surface. The technique addresses the estimation of optimal corresponding points and the corresponding 2D disparity maps leading to the creation of accurate depth perception model.

Keywords: Wavelet transform modulus; Coarse to fine; Disparity; 3D depth

1. Introduction

The 3D reconstruction process can be categorized into three main categories, i.e. calibration: calculating the intrinsic and extrinsic parameters of the cameras [1,2], finding correspondence: finding the corresponding pairs of points projected from the same 3D point on to the two perspective views [3,4], and triangulation: the projection of 2D information back to the 3D space in order to create a 3D depth model [5,6].

A number of algorithms have been proposed to address at least some of these problems in stereo vision [17]. The majority of these algorithms can be categorized into either area based or feature based algorithms. Area

* Corresponding author. Tel.: +61 3 5227 1231; fax: +61 3 5227 1046.
E-mail address: nahavand@deakin.edu.au (S. Nahavandi).

0045-7906/$ - see front matter
doi:10.1016/j.compeleceng.2006.04.003

based approaches [4,19] are based on the correlation of two image functions over locally defined regions. Dense depth maps can be achieved by correlating the grey intensities of image regions in the views being considered assuming that image regions possess some similarities in the perspective views. The area based methods perform well in the presence of rich textured areas but their performance could decline in featureless regions resulting in wrong correspondence [22,23]. Another problem with area based algorithms is their poor performance in handling of surface boundaries, which is very important in the context of generating accurate and dense depth maps [22,23]. On the other hand, feature based algorithms [20,21] attempt to establish correspondences between the selected features, which are extracted using some explicit feature extraction algorithms. The main drawback in these feature based techniques is the retrieval of very sparse depth information making it hard to recover the dense depth maps. The feature based algorithms also have the tendency of getting stuck in unnecessary features of the images and are quite dependent on the efficiency of the feature extraction algorithms.

The main concern in the proposed work is the development of a stereovision algorithm capable of estimating accurate 3D depth of metallic die casting engine parts. The objective is to develop a visual inspection system with minimal hardware involvement unlike many existing techniques which involves the use of laser scanners, laser and light pattern projectors [17,18]. The main motivation behind the algorithm is to keep the system simple, in terms of minimum hardware involvement and complexity, in order to make the system cost effective and cumbersome. Due to its minimal hardware dependency it can be implemented in different factory environments without a significant change in the setup.

Considering the involvement of metallic die casting engine parts with poorly-textured shiny areas and some irregular and unwanted marks, the exclusive use of either area based or feature based algorithms would not be a better choice. Area based algorithms find it hard to estimate the accurate depth in the absence of rich textured image regions whereas feature based algorithms could have difficulty due to the presence of unnecessary and unwanted marks on the surfaces. This escorted us to multiresolution analysis based coarse to fine matching strategy where correspondences are established at different scales and resolutions.

In the context of stereo matching using multiresolution analysis, some work has already been done using scalar wavelets [9,10] and quite promising results have been achieved. The theory of multiwavelets evolved in early 1990s from wavelet theory and was enhanced for more than a decade since then. The success of multiwavelets over scalar wavelet bases stems from the fact that they can simultaneously possess the good properties of orthogonality, symmetry, high approximation order and short support [7,8], which are not possible in the scalar case [7,14]. In this work, multiwavelets based multiresolution approach is used to address the problem of stereo image matching. The presented work is, in fact, a continuation of the work in [11,12]. By using the concept of wavelet transform modulus maxima (**WTMM**) [7] the performance of the algorithm in [12] is improved. It is due to the use of vector coefficients of wavelet transform modulus with magnitude and phase pointing to the normal of the edges.

The rest of the work is organized as the definition of classical wavelet and multiwavelet theory and a brief introduction of **WTMM** is presented in Section 2. Complete disparity estimation process is presented in Section 3 with brief information, explicitly, on similarity measure and consistency check. Results and discussion of different experiments is given in Section 4 followed by the conclusion.

2. Wavelet transform modulus

The classical wavelet theory [7] can be defined by two simple dilation equations as given below

$$\phi(t) = \sum_k c_k \phi(Mt - k) \tag{1}$$

$$\psi(t) = \sum_k w_k \phi(Mt - k) \tag{2}$$

where c_k, w_k are coefficients of scaling functions $\phi(t)$ and wavelets $\psi(t)$, respectively, with M and k representing filter band and integer shifts [24]. Furthermore multiscaling functions $\Phi(t)$ and multiwavelets $\Psi(t)$ can be expressed as

$$\Phi(t) = \begin{bmatrix} \phi_0(t) \\ \phi_1(t) \\ \vdots \\ \phi_{r-1}(t) \end{bmatrix}, \qquad \Psi(t) = \begin{bmatrix} \psi_0(t) \\ \psi_1(t) \\ \vdots \\ \psi_{r-1}(t) \end{bmatrix} \tag{3}$$

where r represents the multiplicity of the multiwavelets which is unity in the case of scalar wavelets. Similarly, in the context of multiwavelets c_k and w_k in (1) and (2) are real $r \times r$ matrices of multi-filter coefficients that iteratively and with rescaling define the scaling and wavelet functions, respectively. The wavelet transform modulus (**WTM**) can then be expressed as

$$\mathrm{WT}_s = |\mathrm{WT}_s| \angle \Theta_W \tag{4}$$

where $|\mathrm{WT}_s|$ represents the magnitude of **WTM**, of kth coefficient, whereas s represents the scale of the subspace. Furthermore, the magnitude of **WTM** can be expressed as

$$|\mathrm{WT}_s| = \sqrt{|W^2_{\mathrm{h},s}| + |W^2_{\mathrm{v},s}|} \tag{5}$$

where $W_{\mathrm{h},s}$ and $W_{\mathrm{v},s}$ are horizontal and vertical detail spaces, respectively. Similarly the phase of the **WTM** can be expressed as

$$\Theta_W = \begin{cases} \alpha(k) & \text{if } W_{\mathrm{h},s} > 0 \\ \pi - \alpha(k) & \text{if } W_{\mathrm{h},s} < 0 \end{cases} \tag{6}$$

where

$$\alpha(k) = \tan^{-1}\left(\frac{W_{\mathrm{v},s}}{W_{\mathrm{h},s}}\right) \tag{7}$$

The vector $\vec{n}(k)$ points to the direction normal to the edge surface as

$$\vec{n}(k) = [\cos(\Theta_W), \sin(\Theta_W)] \tag{8}$$

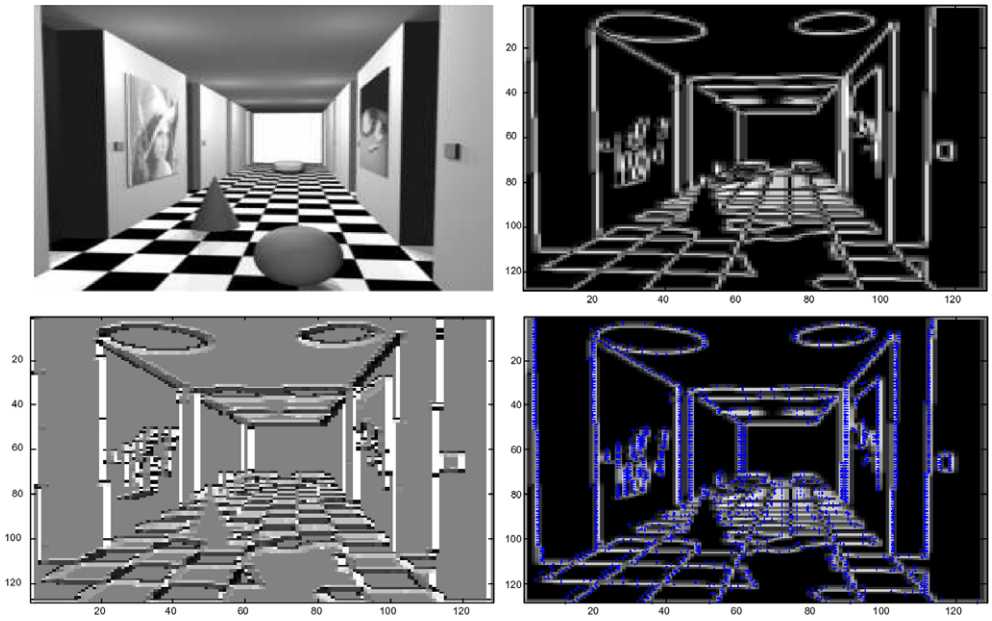

Fig. 1. Top left: original image, top right: wavelet transform modulus, bottom left: wavelet transform modulus phase, bottom right: wavelet transform modulus maxima with phase vectors.

An edge point is the point p at some scale s such that WT_s is locally maximum at $k = p$ and $k = p + \varepsilon\vec{n}(k)$ for $|\varepsilon|$ small enough. These maxima are called wavelet transform modulus maxima **WTMM** [7,13] and are shift invariant. An example of the wavelet transform modulus can be found in Fig. 1 with explicit presentation of magnitude and phase of **WTMM**.

3. Disparity estimation

The matching process starts with scale normalization which minimizes the effect of illuminative variation in each scale that can exist between different scales of perspective views and can be expressed as

$$\mathrm{NW}_s = W_{i,s}/|A_s| \tag{9}$$

where NW_s are the scale normalized wavelet coefficients, i refers to all detail spaces W_i and A_s represents the approximation space within the scale s. After wavelet transformation and the calculation of **WTM**, we end up with coefficient matrices with features highlighted. The scale normalization process is then followed by correlation based similarity measure that can be expressed as

$$C_{x,y,d} = \mathrm{corr}(\mathrm{NW}^1_{s,k}, \mathrm{NW}^2_{s,k}) \quad \text{for } d = 0 \cdots d_{\max} \tag{10}$$

where $\mathrm{NW}^1_{s,k}$ and $\mathrm{NW}^2_{s,k}$ represents normalized **WTMM** related to first and second images, respectively. For more comprehensive visualization of the proposed algorithm a block diagram is shown in Fig. 2.

3.1. Probabilistic weighting

To keep the matching candidates consistent, a symbolic tagging procedure is introduced based on probability of occurrence and three thresholds possessing the criteria $T_1 < T_2 < T_3$. The values of these thresholds is usually within the ranges of [0.5 0.7], [0.70 0.85] and [0.85 0.95], respectively. Theses values of the T_i are carefully chosen by trial and error method. Probability of occurrence P_{oc}, which is the probability of selection of any point as a candidate from any of the search space out of r^2 spaces can be defined as

$$P_{\mathrm{oc}}(C_i) = \frac{n_{C_i}}{r^2} \quad \text{where } 1 \leqslant n_{C_i} \leqslant r^2 \tag{11}$$

Here n_{C_i} is the number of times a candidate match C_i is selected out of search spaces r^2. All matching candidates have equal probability of being selected, i.e. $1/r^2$. The correlation score for each candidate is then weighted with the occurrence probability and can be expressed as

$$PC_i = P_{\mathrm{oc}}(C_i) \sum_n C^i_{x,y,d} \quad \text{where } n \leqslant r^2 \tag{12}$$

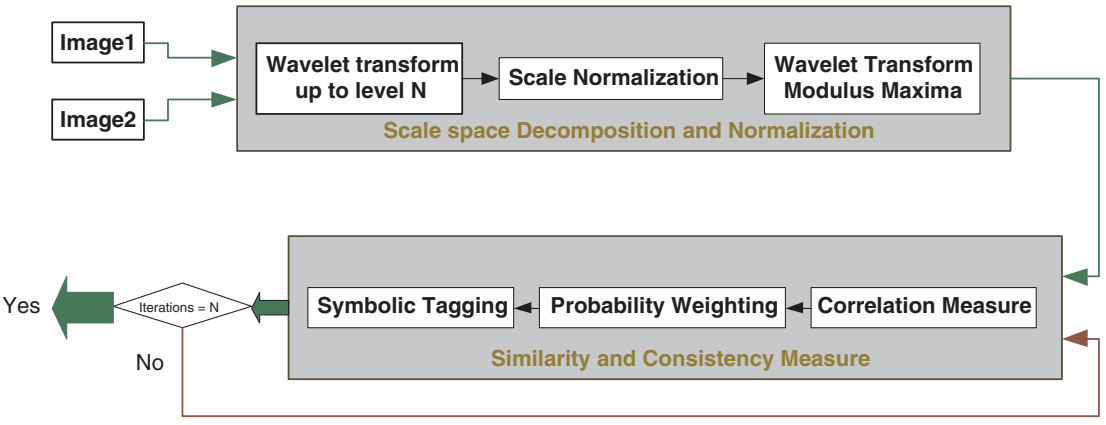

Fig. 2. Block diagram of the proposed algorithm.

3.2. Symbolic tagging

The candidates are then divided into pools based on thresholds T_i. First threshold T_1 is applied just after the correlation step to filter out the bad matches. Remaining candidates are then assigned symbolic tags depending on their consistency as given below

$$\begin{aligned} &C^i_{x,y,d} > T_2, \quad \text{and} \quad PC_i = 1 \Rightarrow \boldsymbol{Op} \\ &C^i_{x,y,d} > T_2, \quad \text{and} \quad 0.5 \leqslant PC_i < 1 \Rightarrow \boldsymbol{Cd} \\ &C^i_{x,y,d} > T_3, \quad \text{and} \quad PC_i < 0.5 \Rightarrow \boldsymbol{Cr} \end{aligned} \tag{13}$$

As can be seen from the first expression, there is no ambiguity for the matches with tag ***Op*** as the probability of consistency is 1, whereas ambiguity does exist for the matches with tags ***Cd*** and ***Cr***. Ambiguity is the phenomenon where there is more than one candidate is available for a single point in the reference image [17,18]. To solve that problem of ambiguity a geometric optimization is performed. The matches fulfilling the geometric topological criteria and having the tag ***Cd*** are then promoted to ***Op*** whereas the ones with the tag ***Cr*** are promoted to ***Cd***. After that step, all matched pairs with the tag ***Op*** are considered as credible matches whereas the matches with the tag ***Cd*** are peer reviewed in the next interpolated level for their credibility. The reason for keeping points with the tag ***Cd*** in consideration is to exploit the possibility of their potential in the next resolution level. The rest of the matches, not fulfilling any of the above criteria, are simply discarded, leaving only the most consistent matches.

3.3. Geometric refinement

As there are r^2 search spaces, there is a possibility of selection of different points from different search spaces, i.e. ambiguity. To address the issue of ambiguity, a simple geometric topological refinement is introduced in order to extract the optimal candidate matches out of the pool of ambiguous candidate matches. For that purpose, the geometric orientation of the ambiguous points with reference to ***Op*** from (13) is checked and the pairs having the closest geometric topology with respect to the ***Op*** are selected as optimal candidates. Three geometric features that are relative distance difference, absolute distance difference and slope difference of lines joining the points were selected and calculated to check the geometric orientational similarity. The geometric measurement is then weighted with the correlation score of candidates to keep the previous achievements of the candidates in the consideration as given below

$$Gc_i = C^i_{x,y,d}\text{ave}\left(e^{-\overline{rd}} + e^{-\overline{ad}} + e^{-\overline{sd}}\right) \tag{14}$$

where $\overline{rd}$, $\overline{ad}$ are the average of relative and absolute distance differences where as $\overline{sd}$ is average slope difference. These geometric features are calculated a number of times in order to minimize the effect of any wrong reference candidate. These three geometric features are invariant through many geometric transformations like Affine, Metric, Euclidean etc. that are very common in the applications of stereo vision and 3D depth estimation [3,6]. The candidate having closest geometric topology, i.e. lowest Gc will be selected as an optimal match.

3.4. Scale interpolation

The matching process at the coarsest level ends up with a number of matching pairs, which needs to be interpolated to the finer level. The constellation relation between the coefficients at coarser and finer levels can be visualized by taking the decimation of factor 2 into consideration though in the case of proposed algorithm averaging is performed, instead, over the consecutive pair of coefficients across rows and columns. The reason of averaging, instead of just discarding every other coefficient by factor 2 decimation, is to keep the significance of all coefficients in consideration. Furthermore there might exist **WTMM** which could be lost by factor 2 decimation instead of averaging. The disparity from coarser disparity d_c to finer disparity d_F can be updated using the relation

$$d_F = d_f + 2d_c \tag{15}$$

where d_f is the estimated disparity at the current scale level.

4. Experiments

The algorithm proposed here is the continuation of the work presented in [11,12] and significant improvements can be observed, regarding the quality of estimated disparity maps. To evaluate the performance of the proposed algorithm, two different kind of experiments are performed. In the first type of experiments, the algorithm in Section 3 is applied to a number of different images taken from Middlebury College's website [15]. These images are well known in the computer vision community due to a variety of texture and intensity based complexities involved in them. The statistical performance check is done by using percentage of bad pixel matches B which can be defined as

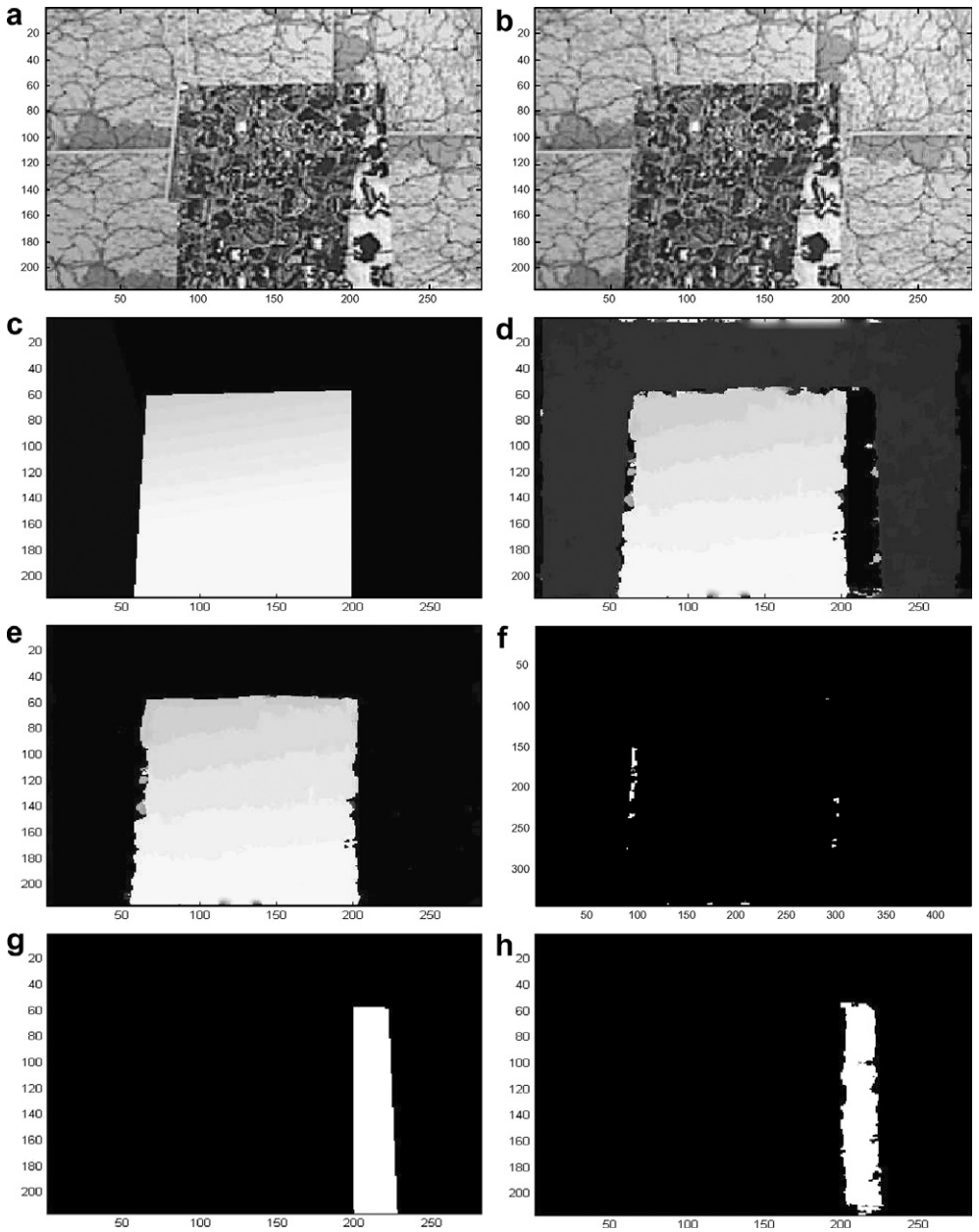

Fig. 3. (a) and (b) Original pair of Map images, (c) ground truth disparity, (d) calculated disparity with occlusion, (e) calculated disparity with occlusion filled, (f) disparity error, (g) occlusion calculated from ground truth, (h) calculated occlusion.

$$B = \frac{1}{N} \sum_{(x,y)} |d_c(x,y) - d_{gth}(x,y)|^2 > \xi \tag{16}$$

where $d_c(x,y)$ and $d_{gth}(x,y)$ represent the calculated and ground-truth disparity maps whereas ξ represents the acceptable disparity difference (usually 0.5). A simple linear interpolation is performed to fill the disparity map gaps where no discrete disparity value could be found, assuming that disparities are found at all discontinuities, i.e. at all wavelet transform modulus maxima.

One of the outcomes of experiments on the images of Middlebury College is shown in Fig. 3 with detailed view and explanation of the disparity estimation and occlusion detection. It seems worth mentioning that no explicit occlusion detection is performed in the proposed algorithm. The detected occluded area is extracted by keeping the matching process highly constrained and promising results were achieved without the involvement of any post optimization procedure. Any match that does not satisfy the consistency checks from Sections 3.1 to 3.3 is simply discarded. It can be seen in Fig. 3(f) where only a few matches were found at the location of occlusion. A simple linear interpolation is then performed by knowing the occlusion region and by the observation that occlusion is on the right side of the higher disparity region. The disparity map after interpolation step is shown in Fig. 3(e) followed by the bad pixel errors in Fig. 3(f). Fig. 3(g) and (h) shows the occluded area related to the ground-truth disparity map shown in Fig. 3(c) and estimated one shown in Fig. 3(d), respectively. The disparity map shown in Fig. 3 is estimated using Chui–Lian multiwavelets bases [14] and is related to right image as right image is taken as a reference image. The calculated error in terms of percentage of bad pixel matches is 2.2%.

The second set of experiments were done on industrial metallic car engine parts. The main motivation behind this project is to develop an algorithm capable of estimating accurate 3D depth of metallic cast engine parts with minimal hardware involvement. The reason is to keep the process simple in terms of hardware complexity so that it can be implemented in different factory environments without a significant change in the setup. As the stereo vision process is not mature enough to solve the problem of depth estimation to high accuracy, external information from a reference 3D model is used. Currently, experiments are performed on metallic pump-covers. The reference model of these pump-covers is produced in Matlab by manually measuring the physical dimensions. In future, 3D reference models from AutoCAD, Solidworks, etc. will also be included as automotive industries usually use these softwares for designing different parts. An example of the reference model, produced in Matlab can be seen in Fig. 4. The information that is needed from the reference image model is the relative location of the discontinuities and the dimensional range of the 3D depth, consequently giving rise to the information regarding the disparity. Relative locations of the different surface edges are the most important as the stereo vision algorithms usually perform poorly in the areas where sharp depth changes occur. It seems wise mentioning here that one reference model is required for each category of objects.

The hardware setup of the presented work is very simple and consists of stereo cameras from Videre Design [16] and simple circular fluorescent light. One example of the estimated depth model is shown in Fig. 5. It can be seen that a very smooth disparity map is obtained after it is optimized and refined using the information extracted from the reference model. One thing that needs to be clarified is that the process is completely inde-

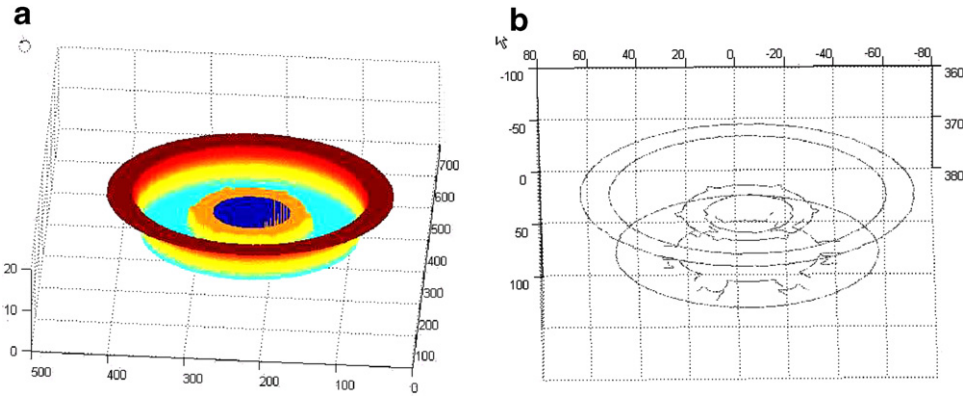

Fig. 4. (a) Reference 3D depth model, (b) surface boundaries.

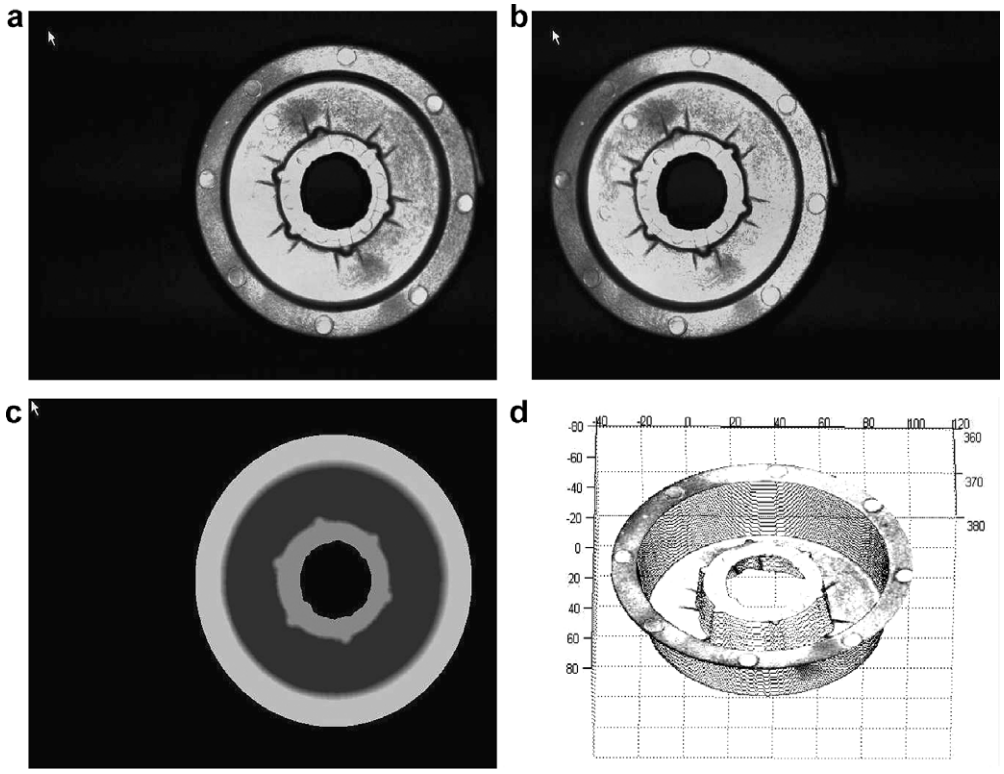

Fig. 5. (a) and (b) Stereo pair of original images, (c) estimated 2D disparity map, (d) 3D depth of model.

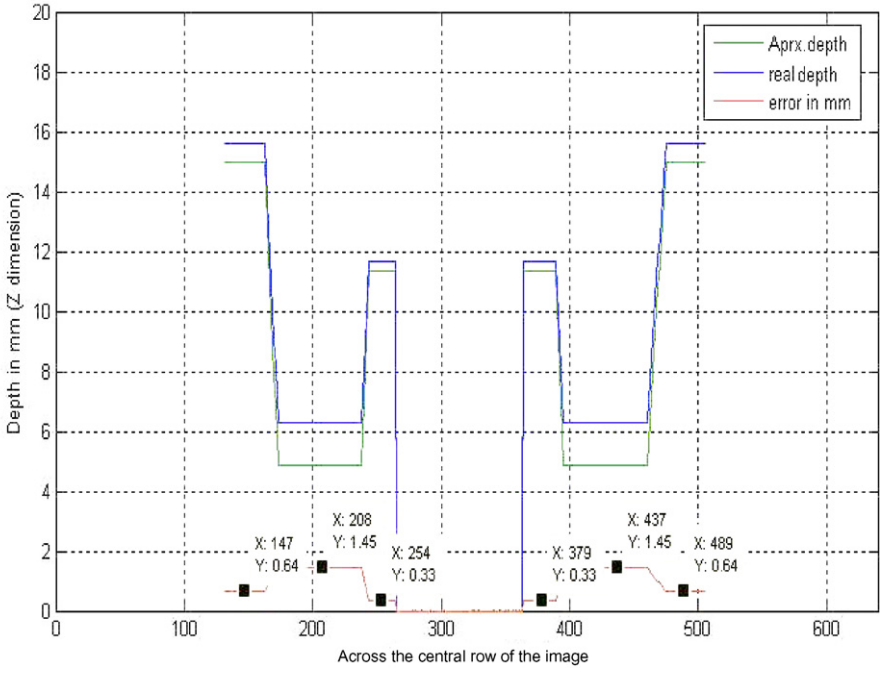

Fig. 6. Error plot between real 3D depth and the recovered one.

pendent of the orientation or the location of the object on the image plane. An error graph is shown in Fig. 6. It shows the difference in depth of different pump-cover surfaces, between the reference depth model as shown in Fig. 4 and estimated one as in Fig. 5(d). It can be seen that error lies within the range of [0.65 mm 1.45 mm], which is very promising considering the simplicity of the proposed algorithm. Furthermore, a series of experiments are underway to check the consistency of the algorithm in a number of different environmental and lighting conditions. The objective is to construct an automated fault detection system using depth information. Complete statistical consistency performance evaluation will be presented in the future evaluating the full capabilities of the algorithm.

5. Conclusion

A multiresolution analysis based stereo vision algorithm is presented. The technique addresses the estimation of optimal corresponding pints consequently leading towards the estimation of accurate 3D depth. The proposed algorithm is a software based approach with minimal hardware involvement. The efficiency and accuracy of the algorithm lies on existing 3D reference model instead of extra hardware tools like laser scanners, laser and light pattern projectors, which makes the system costly and burdensome. Due to its minimal hardware dependency the system is cost effective and can be deployed in different factory environments with different environmental and illuminative variations and without a significant change in the proposed system parameters.

To keep the whole matching process consistent and resistant to errors two techniques, symbolic tagging and geometric refinement, are introduced and are applied along with the common constraints of uniqueness and continuity. The problem of ambiguity explicitly and occlusion implicitly, is addressed using a geometric topological refinement along with the symbolic labeling. Symbolic tagging procedure keeps track of the different candidates and their potentials to be the optimal match by dividing them into different bins based on the probability of occurrence and threshold levels. The tags of the candidates update with their performances and potential along the procedure instead of just discarding the matches who does not follow the criteria of fixed thresholds as in the winner takes all strategies.

Acknowledgements

This work was supported by the Cooperative Research Centre for Cast Metals Manufacturing (CAST). CAST was established and is funded in part by the Australian Government's Cooperative Research Centre Program.

References

[1] Zhang Z. A flexible new technique for camera calibration. IEEE Trans Pattern Anal Machine Intell 2000;22(11):1330–4.
[2] Molton ND, Davison AJ, Reid ID. Parameterisation and probability in image alignment. In: Proc Asian conference on computer vision, 2004.
[3] Faugeras O, Luong QT, Papadopoulo T. The geometry of multiple images. MIT Press; 2001.
[4] Zhang Z, Deriche R, Faugeras O, Luong QT. A robust technique for matching two uncalibrated images through the recovery of the unknown epipolar geometry. In: Research report 2273, INIRA, Sophia-Antipolis, 1994.
[5] Hartley R. Triangulation. Comput Vision Image Understanding 1997;68(2):146–57.
[6] Hartley R, Zisserman A. Multiple view geometry. 2nd ed. Cambridge, UK: Cambridge University Press; 2003.
[7] Mallat S. A wavelet tour of signal processing. Harcourt Place, London: Academic Press; 2001.
[8] Özkaramanli H, Bhatti A, Bilgehan B. Multi wavelets from B-Spline super functions with approximation order. Signal Process 2002;82(9):1029–46.
[9] He-Ping Pan. Uniform full-information image matching using complex conjugate wavelet pyramids. In: XVIII ISPRS Congress, International Archives of Photogrammetry and Remote Sensing, 1996.
[10] He-Ping Pan. General stereo matching using symmetric complex wavelets. In: Wavelet applications in signal and image processing, vol. 2825; 1996.
[11] Asim Bhatti, Saeid Nahavandi, Hong Zheng. Image matching using TI multi-wavelet transform. In: Digital image computing techniques and application, 2003. p. 937–46.
[12] Asim Bhatti, Saeid Nahavandi. A multi-wavelet based technique for calculating dense 2D disparity maps from stereo. In: World automation congress, 2004.
[13] Mallat S, Zhang S. Matching pursuits with time–frequency dictionaries. IEEE Trans Signal Process 1993;41(12):3397–415.

[14] Chui CK, Lian J. A study of orthonormal multi-wavelets. J Appl Numer Math 1996;20(3):273–98.
[15] Scharstein D, Szeliski R. Middlebury college stereo vision research page. Available from: http://www.middlebury.edu/stereo.
[16] Available from: http://www.videredesign.com/.
[17] Scharstein D, Szeliski R. A taxonomy and evaluation of dense two-frame stereo correspondence algorithms. Intl J Comput Vision 2002;47(1):8–42.
[18] Scharstein D, Szeliski R. High-accuracy stereo depth maps using structured light. In: IEEE computer society conference on computer vision and pattern recognition (CVPR 2003), vol. 1; 2003. p. 195–202.
[19] Di Stefano L, Mattoccia MMS, Neri G. A fast area-based stereo matching algorithm. Image Vision Comput 2004;22(13):938–1005.
[20] Huang TS, Netravali AN. Motion and structure from feature correspondences: a review. In: Proc of the IEEE, 1994.
[21] Tommasini T, Trucco AFE, Roberto V. Making good features track better. In: Proc IEEE Conf on Computer Vision and Pattern Recognition, 1998.
[22] Hirschmuller H, editor. Improvements in real-time correlation-based stereo vision in workshop on stereo and multi-baseline vision. Kauai, Hawaii: IEEE; 2001.
[23] Muhlmann K, Maier D, Hesser J, Manner R. Calculating dense disparity maps from color stereo images, an efficient implementation. In: IEEE workshop on stereo and multi-baseline vision, 2001.
[24] Strang G, Nguyen T. Wavelets and filter banks. Wellesley-Cambridge Press; 1996.

Asim Bhatti has received his BS and MS degrees from the Eastern Mediterranean University, North Cyprus Turkey, and PhD from Deakin University, Australia in 2005. He has joined Deakin University as a Research Academic in 2005 where he is conducting research in Computer/Machine Vision, Augmented Reality, Robotics and Haptics. Asim Bhatti has published over 10 peer-reviewed papers in the areas of Computer/Machine vision and image/signal processing.

Saeid Nahavandi received BSc (Hons), MSc and a PhD from Durham University (UK). In 1991 he joined Massey University (NZ) where he taught and led research in robotics as a Senior Lecturer. In 1998 he became an Associate Professor at Deakin University (AU) and the leader for the Intelligent Systems research group and also Manager for the Cooperative Research Center for CAST Metals Manufacturing. In 2002 Professor Nahavandi took the position of Chair in Engineering in the same university. Dr. Nahavandi has published over 190 reviewed papers and delivered several invited plenary lectures at international conferences. He is the recipient of four international awards, best paper award at the World Automation Congress (USA) and the Young Engineer of the Year award. Professor Nahavandi is the founder of the World Manufacturing Congress series and the Autonomous Intelligent Systems Congress series. He is a Fellow of IEAust and IEE. His current research interests include modeling and control and the application of soft computing to industrial processes.

Yakov Frayman has received MSc degree from the State Polytechnic Academy of Belarus, MEng degree from Victoria University of Technology, Australia, and a PhD from Deakin University, Australia. After working for more than 20 years in manufacturing in the area of Industrial Control and Automation, in 2000 he has joined Deakin University as a Research Academic where he is conducting research in neural networks, machine learning, data mining and machine vision. Dr. Frayman has published over 30 peer-reviewed papers in the areas of intelligent modeling and control and the applications of soft computing to manufacturing.